Robotica (2012) volume 30, pp. 195–203. © Cambridge University Press 2011
doi:10.1017/S0263574711000518

Two-state trajectory tracking control of a spherical robot using neurodynamics

Yao Cai*, Qiang Zhan and Caixia Yan

Robotics Institute, Beijing University of Aeronautics and Astronautics, Beijing, 100191, China

(Received in Final Form: May 10, 2011; accepted May 6, 2011. First published online: June 6, 2011)

SUMMARY

Spherical robot is a special kind of nonholonomic system that cannot be converted to chained form, which means most of the well-known control methodologies are not suitable for this system. For the trajectory tracking of BHQ-1, a spherical robot designed by our lab, a two-state trajectory tracking controller is proposed in this paper. First, the kinematic model of the robot is built using screw theory and exponential method and the controllability is proved based on the differential geometric control theory. Then to solve the two-state trajectory tracking problem of BHQ-1, a shunting model of neurodynamics and Lyapunov's direct method are combined to design a two-state trajectory tracking controller, of which the Lyapunov stability is validated. Finally, typical simulation examples, such as tracking linear, circular, and sinusoidal trajectories, are introduced to verify the effectiveness of the proposed controller. In this paper the proposed method can also be applied to the control of other spherical robots.

KEYWORDS: Spherical Robot; Trajectory Tracking; Neurodynamics; Kinematics Modeling; Nonholonomic Systems.

1. Introduction

Spherical robot is a new type of mobile robot that has a ball-shaped outer shell to include all its mechanism, control devices, and energy sources in it. Spherical robots belong to nonholonomic system, but they cannot be converted into chained form.[1] There are still no proven general control methodologies for spherical robots, although some control methods were proposed. Li and Canny[2] proposed a three-step algorithm to solve the motion planning problems of a sphere, the position coordinates of the sphere are converged to the desired values in three steps. This method is complete in theory, but it cannot be applied to spherical robot like BHQ-1 that cannot turn with zero radius as the configurations are constrained. Mukherjee and Das *et al.*[3,4] proposed a feedback stabilization algorithm for four-dimensional reconfiguration of a sphere. However, the algorithm needs numerous operations to converge to the desired values. By considering a spherical robot as a chained system, Javadi and Mojabi[5] established its dynamic model with the Newton method and discussed its motion planning. Simulations and experiments were done in a small moving scale and showed poor moving accuracy. Bhattacharya and Agrawal[6] deduced the first-order mathematical model of a kind of spherical robot from the nonslip constraint and angular momentum conservation and discussed the problems of trajectory planning with minimum energy and time. Halme *et al.*[7,8] analyzed the rolling ahead motion of a spherical robot with dynamic equation, but they did not consider the steering motion. Bicchi *et al.*[9,10] established a simplified dynamic model for a spherical robot and discussed its motion planning on a plane with obstacles, but they did not discuss the path following and trajectory tracking problems. Joshi *et al.*[11,12] deduced the kinematics model of a spherical robot using Euler parameters and demonstrated its controllability. With the Lagrangian equation, Liu *et al.*[13] deduced a simplified dynamic model of a spherical robot by input-state linearization. Using the Lagrange-d'Alembert formula Zhan *et al.*[14] deduced the dynamic model of BHQ-1 spherical robot based on the quasi-velocity, but did not discuss the path following and trajectory tracking problems.

As discussed above, the present control research of spherical robots mainly focuses on the modeling, stabilization, and motion planning, whereas the trajectory tracking problem, which is more useful in practice, is rarely discussed.

This paper proposed a control method to solve the two-state trajectory tracking problem of a spherical robot BHQ-1, which is developed for research and environment exploration by our lab. The remainder of the paper is structured as follows: In Section 2, the kinematic model of BHQ-1 is deduced. In Section 3, a two-state trajectory tracking controller based on Lyapunov's direct method and neurodynamics technique is proposed. The simulation results are presented in Section 4. Finally, conclusions are given in Section 5.

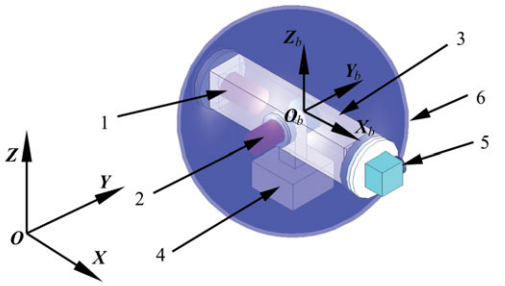
2. Kinematic Modeling and Controllability Analysis

The mechanical structure of BHQ-1 is illustrated in Fig. 1. BHQ-1 consists of two motors, a hollow shaft, a mass, a camera, and a shell. The hollow shaft connected with the shell through ball bearings serves as a frame to install other devices. The output axle of motor 1 is fixed to the shell; the output axle of motor 2 is fixed to the mass by a link. The camera can be used to take pictures of environments.

The moving principle of spherical robot BHQ-1 is as follows. When motor 1 rotates around axis X_b and motor

* Corresponding author. E-mail: caiyao1985@me.buaa.edu.cn

https://doi.org/10.1017/S0263574711000518 Published online by Cambridge University Press



1 — Motor 1, 2 — Motor 2, 3 — Hollow shaft,
4 — Mass, 5 — Camera, 6 — Shell

Fig. 1. (Colour online) Structure of spherical robot BHQ-1.

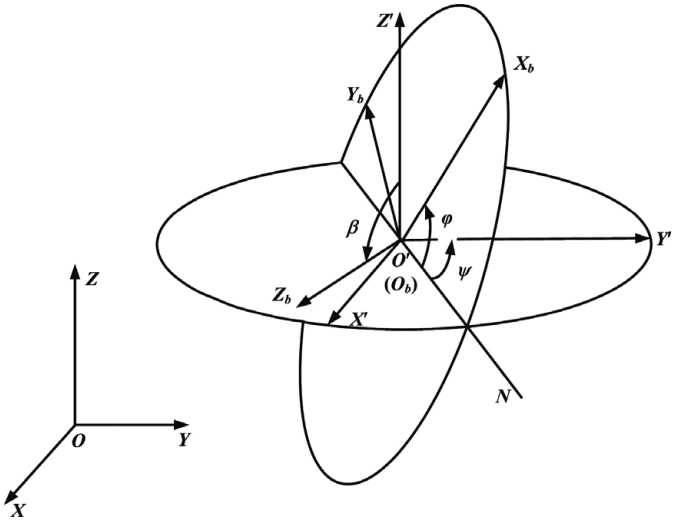


Fig. 2. Pose of spherical robot BHQ-1.

2 keeps static, the rotation of the mass and the hollow shaft around axis X_b change gravity center of the robot and produce a gravity torque that makes the robot move forward or backward. When both motor 1 and motor 2 rotate, the mass and the hollow axle will tilt and produce a gravity torque to veer the robot. Consequently, drived by two motors, the spherical robot can move and veer as anticipated. Therefore, we can control the motion of the robot through the controlling of two motors.

In this section, we derive the kinematic model of BHQ-1 using screw theory and prove its controllability with differential geometry method. It has also been proven that the kinematic model of BHQ-1 cannot be transformed into a chained form.

2.1. Kinematic modeling

The kinematic model of spherical robot BHQ-1 is derived on the basis of the following assumptions:

1. The spherical shell is rigid.
2. The spherical shell rolls without slipping on the ground.
3. Rotations of the sphere around the vertical axis are ignored.

The pose of spherical robot BHQ-1 is shown in Fig. 2.

There are three right-hand coordinate frames: $OXYZ$, $O'X'Y'Z'$, and $O_bX_bY_bZ_b$. The relationships between these three coordinate frames can be described as follows:

1. $OXYZ$ is an absolute or reference coordinate frame fixed to the ground.
2. O_b and O' are coincident with the spherical center.
3. $O'X'Y'Z'$ is parallel to $OXYZ$.
4. $O_bX_bY_bZ_b$ is fixed to the robot.

It can be considered that the spherical robot has three rotation axes: X_b, Y_b, and Z_b. In order to describe the pose of BHQ-1, we use three ZYX Euler angles ψ, β, and φ. Then three twists of the robot in the coordinate frame $O'X'Y'Z'$ can be expressed, respectively, as

$$\begin{cases} \boldsymbol{\xi}_{\psi} = [0,0,0,0,0,1]^T, \\ \boldsymbol{\xi}_{\beta} = [0,0,0,0,1,0]^T, \\ \boldsymbol{\xi}_{\varphi} = [0,0,0,1,0,0]^T. \end{cases} \tag{1}$$

The exponential of these three twists can be given as

$$\begin{cases} e^{\hat{\boldsymbol{\xi}}_{\psi}\psi} = \begin{pmatrix} \cos\psi & -\sin\psi & 0 & 0 \\ \sin\psi & \cos\psi & 0 & 0 \\ 0 & 0 & 1 & 0 \\ 0 & 0 & 0 & 1 \end{pmatrix}, \\ e^{\hat{\boldsymbol{\xi}}_{\beta}\beta} = \begin{pmatrix} \cos\beta & 0 & \sin\beta & 0 \\ 0 & 1 & 0 & 0 \\ -\sin\beta & 0 & \cos\beta & 0 \\ 0 & 0 & 0 & 1 \end{pmatrix}, \\ e^{\hat{\boldsymbol{\xi}}_{\varphi}\varphi} = \begin{pmatrix} 1 & 0 & 0 & 0 \\ 0 & \cos\varphi & -\sin\varphi & 0 \\ 0 & \sin\varphi & \cos\varphi & 0 \\ 0 & 0 & 0 & 1 \end{pmatrix}. \end{cases} \tag{2}$$

The instantaneous velocity of the robot in $O'X'Y'Z'$ is given by the twist[1]

$$\boldsymbol{V}_{O'} = \boldsymbol{J}_{O'}(\boldsymbol{\theta})\boldsymbol{\theta}', \tag{3}$$

where,

$$\begin{cases} \boldsymbol{\theta} = [\psi, \beta, \varphi]^T, \\ \boldsymbol{J}_{O'} = [\boldsymbol{\xi}_{\psi}, \boldsymbol{\xi}'_{\beta}, \boldsymbol{\xi}'_{\varphi}], \\ \boldsymbol{\xi}'_{\beta} = \mathrm{Ad}_{e^{\hat{\boldsymbol{\xi}}_{\psi}\psi}}\boldsymbol{\xi}_{\beta}, \\ \boldsymbol{\xi}'_{\varphi} = \mathrm{Ad}_{e^{\hat{\boldsymbol{\xi}}_{\psi}\psi}e^{\hat{\boldsymbol{\xi}}_{\beta}\beta}}\boldsymbol{\xi}_{\varphi}, \end{cases} \tag{4}$$

and

$$\begin{cases} \mathrm{Ad}_g : \Re^6 \to \Re^6 = \begin{pmatrix} \boldsymbol{R} & \hat{\boldsymbol{p}}\boldsymbol{R} \\ \boldsymbol{0} & \boldsymbol{R} \end{pmatrix}, \\ \boldsymbol{g} = \begin{pmatrix} \boldsymbol{R} & \boldsymbol{p} \\ 0 & 1 \end{pmatrix} \in \boldsymbol{SE}(3). \end{cases} \tag{5}$$

Substituting Eqs. (1) and (2) into Eq. (4), we get

$$\boldsymbol{V}_{O'} = \begin{pmatrix} \boldsymbol{v}_{O'} \\ \boldsymbol{\omega}_{O'} \end{pmatrix} = \begin{pmatrix} 0 \\ 0 \\ 0 \\ -\beta'\sin\psi + \varphi'\cos\psi\cos\beta \\ \beta'\cos\psi + \varphi'\sin\psi\cos\beta \\ \psi' - \varphi'\sin\beta \end{pmatrix}, \tag{6}$$

https://doi.org/10.1017/S0263574711000518 Published online by Cambridge University Press

where, $\boldsymbol{v}_{O'}$ and $\boldsymbol{\omega}_{O'}$ are translational velocity and angular velocity of the robot in $O'X'Y'Z'$, respectively; φ', β', and ψ' denote the time derivative of φ, β, and ψ, respectively. According to the assumptions and relationships among these three coordinate frames, the velocity of the robot in the absolute coordinate frame *OXYZ* can be derived as

$$\begin{cases} \omega_x = -\beta' \sin\psi + \varphi' \cos\psi \cos\beta \\ \omega_y = \beta' \cos\psi + \varphi' \sin\psi \cos\beta \\ \omega_z = 0 \quad \Rightarrow \quad \psi' = \varphi' \sin\beta \\ v_x = R\omega_y = R\beta' \cos\psi + R\varphi' \sin\psi \cos\beta \\ v_y = -R\omega_x = R\beta' \sin\psi - R\varphi' \cos\psi \cos\beta \\ v_z = 0 \end{cases}, \tag{7}$$

where, v_x, v_y, and v_z are absolute translational velocity components along axes X, Y, and Z, respectively; ω_x, ω_y, and ω_z are absolute angular velocity components around axes X, Y, and Z, respectively; and R is the radius of the spherical shell.

Let $\boldsymbol{p} = [x, y, \psi, \beta, \varphi]^T$ denote the configuration of the spherical robot, where (x, y) denotes the position of the spherical center and (ψ, β, φ) describes the orientation of the robot with three Euler angles. Converting Eq. (7) to a control system by choosing the driving velocity φ' and the steering velocity β' as inputs gives

$$\boldsymbol{p}' = \boldsymbol{g}_1(p)\varphi' + \boldsymbol{g}_2(\boldsymbol{p})\beta', \tag{8}$$

where

$$\boldsymbol{g}_1(\boldsymbol{p}) = \begin{pmatrix} R\sin\psi\cos\beta \\ -R\cos\psi\cos\beta \\ 1 \\ 0 \\ \sin\beta \end{pmatrix}, \quad \boldsymbol{g}_2(\boldsymbol{p}) = \begin{pmatrix} R\cos\psi \\ R\sin\psi \\ 0 \\ 1 \\ 0 \end{pmatrix}.$$

Under the mechanical constraints of BHQ-1, β can vary over a range of $-\pi/2$ to $\pi/2$.

2.2. *Controllability analysis*

Let $[\boldsymbol{f}, \boldsymbol{g}]$ denote the Lie bracket between two vector fields,

$$[\boldsymbol{f}, \boldsymbol{g}] = \frac{\partial \boldsymbol{g}}{\partial \boldsymbol{p}}\boldsymbol{f} - \frac{\partial \boldsymbol{f}}{\partial \boldsymbol{p}}\boldsymbol{g}, \tag{9}$$

then the controllability filtration of the nonlinear control system (8) is defined as the following iterative sequence of distributions[18]

$$\begin{cases} \Delta_0 = \Delta, \\ \Delta_1 = \Delta_0 + [\Delta_0, \Delta_0], \\ \Delta_2 = \Delta_1 + [\Delta_1, \Delta_0], \\ \vdots \\ \Delta_{i+1} = \Delta_i + [\Delta_i, \Delta_0], \end{cases} \tag{10}$$

where $\boldsymbol{\Delta} = span\{\boldsymbol{g}_1(\boldsymbol{p}),$ and $\boldsymbol{g}_2(\boldsymbol{p})\}$ is the input distribution.

Constructing the filtration, we have

$$\begin{aligned} \boldsymbol{g}_3 &= [\boldsymbol{g}_1, \boldsymbol{g}_2] \\ &= [0, 0, 0, 0, -\cos\beta]^T. \\ \boldsymbol{g}_4 &= [\boldsymbol{g}_1, \boldsymbol{g}_3] \\ &= [R\cos^2\beta\cos\psi, R\cos^2\beta\sin\psi, 0, 0, 0]^T. \\ \boldsymbol{g}_5 &= [\boldsymbol{g}_2, \boldsymbol{g}_3] \\ &= [-R\cos\beta\sin\psi, R\cos\beta\cos\psi, 0, 0, \sin\beta]^T. \\ \Delta_0 &= span\{\boldsymbol{g}_1, \boldsymbol{g}_2\}, \mathbf{dim}\Delta_0 = 2. \\ \Delta_1 &= span\{\boldsymbol{g}_1, \boldsymbol{g}_2, \boldsymbol{g}_3\}, \mathbf{dim}\Delta_1 = 3. \\ \Delta_2 &= span\{\boldsymbol{g}_1, \boldsymbol{g}_2, \boldsymbol{g}_3, \boldsymbol{g}_4, \boldsymbol{g}_5\}, \mathbf{dim}\Delta_2 = 5 \end{aligned}$$

For all $\boldsymbol{p}$ $(-\pi/2 < \beta < \pi/2)$, Δ_2 is full rank and hence the spherical robot BHQ-1 is controllable and has a degree of nonholonomy 3 with growth vector (2, 3, 5). The relative growth vector for this system is (2, 1, 2). The necessary condition for a system to convert to a chained form[1] is $\mathbf{dim}\Delta_i = i + 2$. According to the above computation, the kinematic model of spherical robot BHQ-1 cannot be converted to a chained form.

3. Trajectory Tracking

Motivated by Lyapunov's direct method and biological neurodynamic techniques, we proposed a two-state trajectory tracking controller for spherical robot BHQ-1. A shunting model is used as a neurodynamic model to govern the dynamics of control variables. In order to simplify the tracking problem, only continuous trajectories are considered. Also provided in this section is the Lyapunov stability analysis.

3.1. *Shunting model*

Hodgkin and Huxley[16] proposed a model for a patch of membrane in a biological neural system using electrical circuit elements, which provides the foundation of the shunting model and leads to a lot of varied models and applications. A typical shunting equation derived from Hodgkin and Huxley's membrane model[16] is described by

$$\frac{\mathrm{d}\zeta}{\mathrm{d}t} = -A\zeta + (B - \zeta)S(t)^+ - (D + \zeta)S(t)^-, \tag{11}$$

where, ζ is the neural activity (membrane potential) of the neuron; A, B, and D are nonnegative constants representing the passive decay rate, the upper and lower bounds of the neural activity, respectively; S^+ and S^- are the excitatory and inhibitory inputs to the neuron, respectively. The state responses of the models are limited to the finite interval $(-D, B)$, and the stability and convergence of the model were rigorously proved by the Lyapunov stability theory.[17]

3.2. *Tracking algorithm*

Two configuration states such as position (x, y) are controlled to track desired values, while the orientation of the robot is not considered. As long as the reference trajectory is non-stationary and position variables are involved in the control, the vehicle's orientation is stable.[15]

https://doi.org/10.1017/S0263574711000518 Published online by Cambridge University Press

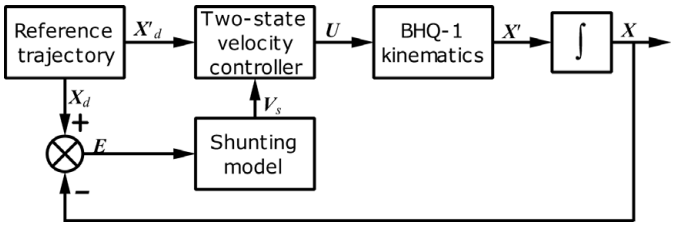


Fig. 3. Scheme of the proposed two-state tracking controller of BHQ-1.

The two-state trajectory tracking problem can be described by

$$\boldsymbol{X}' = \boldsymbol{A}\boldsymbol{U}, \tag{12}$$

where, $\boldsymbol{X} = [x, y]^T$,

$$\boldsymbol{A} = \begin{pmatrix} R\sin\psi\cos\beta & R\cos\psi \\ -R\cos\psi\cos\beta & R\sin\psi \end{pmatrix},$$
$$\boldsymbol{U} = [u_1, u_2]^T = [\varphi', \beta']^T.$$

Given the reference trajectory $\boldsymbol{X}_d = [x_d, y_d]^T$, we can get the tracking error as

$$\boldsymbol{E} = \boldsymbol{X}_d - \boldsymbol{X} = [e_x, e_y]^T, \tag{13}$$

where $e_x = x_d - x$ and $e_y = y_d - y$ are the position errors between the real robot trajectory and the reference trajectory x_d and y_d.

The schematic diagram of the real-time trajectory tracking controller of the spherical robot BHQ-1 is shown in Fig. 3, which includes a velocity controller with a biological neuron for kinematics control of BHQ-1.

Considering the following Lyapunov function candidate,

$$\Gamma = \frac{1}{2}\boldsymbol{E}^T\boldsymbol{E}, \tag{14}$$

the time derivative of Γ is

$$\begin{aligned}\Gamma' &= \boldsymbol{E}^T\boldsymbol{E}' = \boldsymbol{E}^T\left(\boldsymbol{X}'_d - \boldsymbol{X}'\right), \\ &= \boldsymbol{E}^T\left(-\boldsymbol{A}\boldsymbol{U} + \boldsymbol{X}'_d\right),\end{aligned} \tag{15}$$

where, $\boldsymbol{E}'$, $\boldsymbol{X}'_d$, and $\boldsymbol{X}'$ represent the time derivative of $\boldsymbol{E}$, $\boldsymbol{X}_d$, and $\boldsymbol{X}$, respectively. If the control law is chosen as

$$\boldsymbol{U} = \boldsymbol{A}^{-1}(\boldsymbol{\Lambda}\boldsymbol{E} + \boldsymbol{X}'_d), \tag{16}$$

where $\boldsymbol{\Lambda} \in \boldsymbol{GL}(2, \Re)$ is positive definite. Equation (15) becomes

$$\Gamma' = -\boldsymbol{E}^T\boldsymbol{\Lambda}\boldsymbol{E}, \tag{17}$$

$\Gamma' \leq 0$ and $\Gamma' = 0$ if and only if $\boldsymbol{E} = 0$. Therefore, the system is globally, asymptotically stable.

By analyzing the controller in Eq. (16), initially, if $\boldsymbol{E} \neq 0$, then $\varphi' \neq 0$ and $\beta' \neq 0$, that is to say, the speed jump happens. Besides, this controller produces discontinuous control outputs, and results in sudden speed change, which cannot happen in the real world. Due to the characteristics of the shunting model discussed above, the output of the shunting model is bounded in a finite interval and smooth without any sharp jumps when inputs have sudden changes. In order to solve the speed jump problem caused by an initial position error, the shunting model is fused in the above controller when it tracks a continuous path. The following control algorithm is proposed to deal with the continuous trajectory tracking problem.

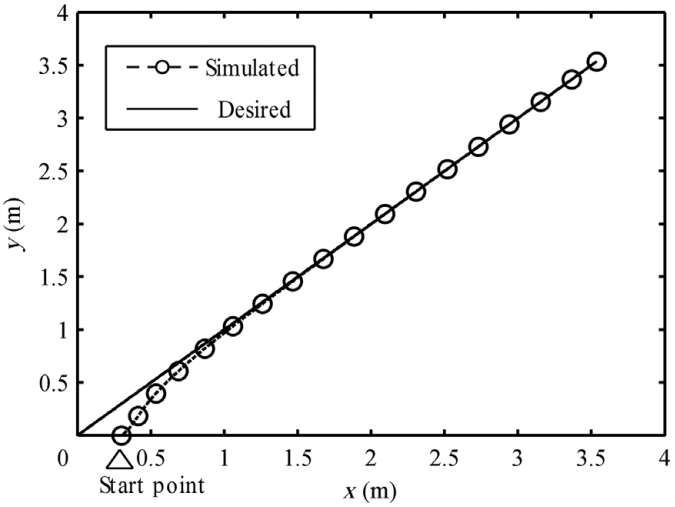


Fig. 4. Spherical robot BHQ-1 tracking a linear trajectory.

$$\boldsymbol{U} = \boldsymbol{A}^{-1}(\boldsymbol{V}_s + \boldsymbol{X}'_d) \tag{18}$$

In Eq. (18), $\boldsymbol{V}_s = [V_{sx}, V_{sy}]^T$ are functions of the shunting model as

$$\boldsymbol{V}'_s = \left[V'_{sx}, V'_{sy}\right]^T,$$
$$\begin{cases} V'_{sx} = -AV_{sx} + (B - V_{sx})f(e_x) - (D + V_{sx})g(e_x), \\ V'_{sy} = -AV_{sy} + (B - V_{sy})f(e_y) - (D + V_{sy})g(e_y), \end{cases} \tag{19}$$

where $\boldsymbol{V}'_s$ denotes the time derivative of $\boldsymbol{V}_s$; $f(e_x) = \max(e_x, 0)$; and $g(e_y) = \max(-e_y 0)$.

3.3. Stability analysis

Considering the following Lyapunov function candidate,

$$\Gamma = \frac{1}{2}\boldsymbol{E}^T\boldsymbol{E} + \frac{1}{2B}\boldsymbol{V}_s^T\boldsymbol{V}_s, \tag{20}$$

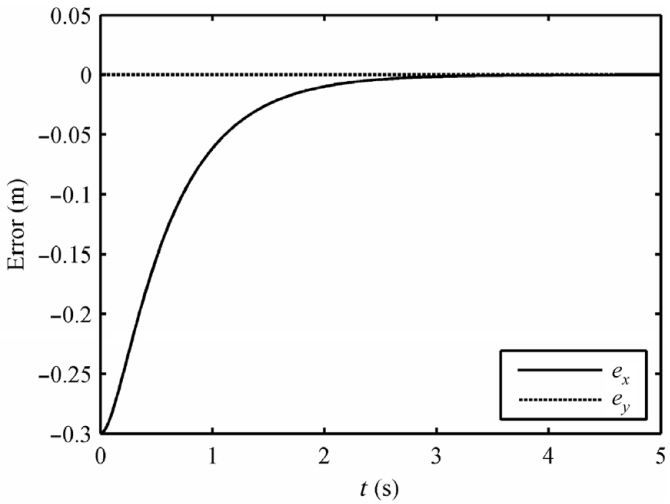
where Γ is a positive definite function if and only if $\boldsymbol{E} = 0$ and $\boldsymbol{V}_s = 0$, and $\Gamma = 0$; otherwise, $\Gamma > 0$. The time derivative of Γ can be derived as

$$\Gamma' = \boldsymbol{E}^T\boldsymbol{E}' + \boldsymbol{V}_s^T\boldsymbol{V}'_s. \tag{21}$$

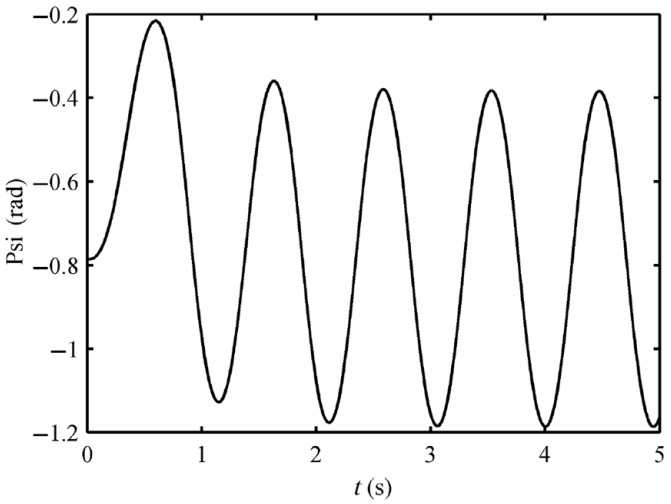
For the first term of Eq. (21), we can get

$$\begin{aligned}\boldsymbol{E}^T\boldsymbol{E}' &= \boldsymbol{E}^T(\boldsymbol{X}'_d - \boldsymbol{X}'), \\ &= \boldsymbol{E}^T(\boldsymbol{X}'_d - \boldsymbol{A}\boldsymbol{U}).\end{aligned} \tag{22}$$

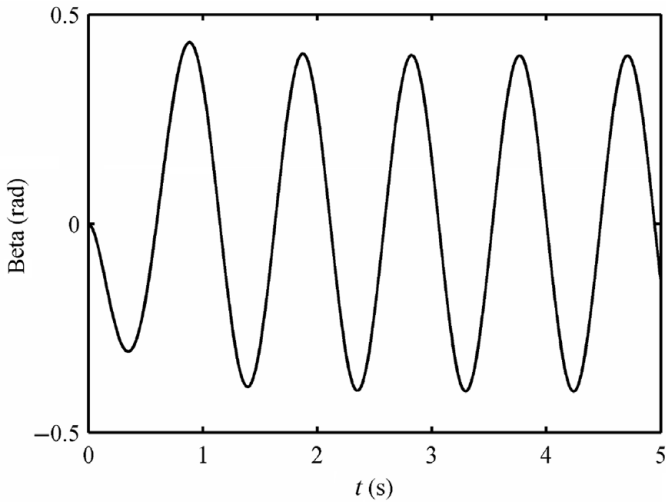
https://doi.org/10.1017/S0263574711000518 Published online by Cambridge University Press



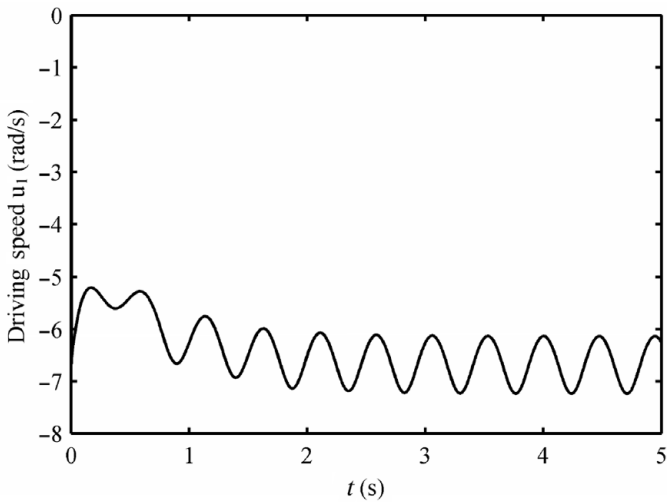
(a) Tracking errors e_x, e_y



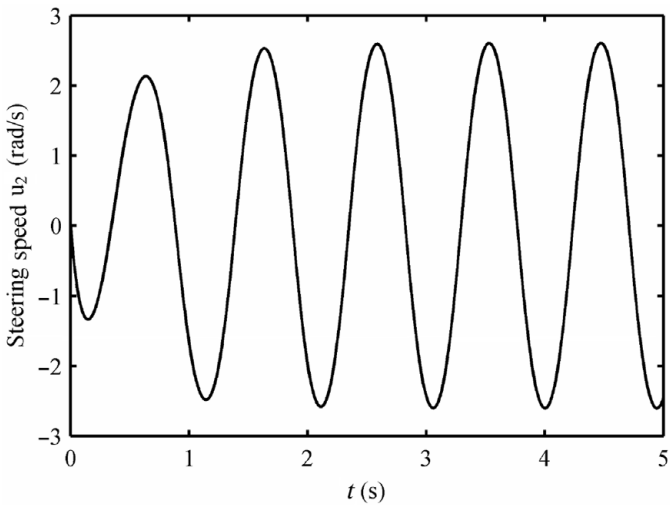
(b) Attitude angle ψ



(c) Attitude angle β



(d) Driving speed φ'



(e) Steering speed β'

Fig. 5. Tracking errors, attitude angles, and velocities for a linear trajectory.

https://doi.org/10.1017/S0263574711000518 Published online by Cambridge University Press

Substituting $\boldsymbol{U}$ from Eq. (18), we have

$$\begin{aligned}\boldsymbol{E}^T\boldsymbol{E}' &= \boldsymbol{E}^T\left[\boldsymbol{X}_d' - \boldsymbol{A}\boldsymbol{A}^{-1}\left(\boldsymbol{V}_s + \boldsymbol{X}_d'\right)\right], \\ &= -\boldsymbol{E}^T\boldsymbol{V}_s = -(e_x V_{sx} + e_y V_{sy}).\end{aligned} \tag{23}$$

The second term of Eq. (21) is given as

$$\begin{aligned}\boldsymbol{V}_s^T\boldsymbol{V}_s' = &-\frac{1}{B}\left[A + f(e_x) + g(e_x)\right]V_{sx}^2 \\ &-\frac{1}{B}\left[A + f(e_y) + g(e_y)\right]V_{sy}^2 \\ &+\frac{1}{B}\left[Bf(e_x) - Dg(e_x)\right]V_{sx} \\ &+\frac{1}{B}\left[Bf(e_y) - Dg(e_y)\right]V_{sy}.\end{aligned} \tag{24}$$

If $B = D$, then

$$\begin{aligned}\boldsymbol{V}_s^T\boldsymbol{V}_s' = &-\frac{1}{B}\left[A + f(e_x) + g(e_x)\right]V_{sx}^2 \\ &-\frac{1}{B}[A + f(e_y) + g(e_y)]V_{sy}^2 \\ &+[f(e_x) - g(e_x)]V_{sx} \\ &+[f(e_y) - g(e_y)]V_{sy}.\end{aligned} \tag{25}$$

Equation (21) becomes

$$\begin{aligned}\Gamma' = &-\frac{1}{B}\left[A + f(e_x) + g(e_x)\right]V_{sx}^2 \\ &-\frac{1}{B}\left[A + f(e_y) + g(e_y)\right]V_{sy}^2 \\ &+\left[f(e_x) - g(e_x) - e_x\right]V_{sx} \\ &+\left[f(e_y) - g(e_y) - e_y\right]V_{sy}.\end{aligned} \tag{26}$$

According to the definitions of $f(e_x)$ and $g(e_x)$, if $e_x \geq 0$, $f(e_x) = e_x$, and $g(e_x) = 0$, then

$$\begin{cases}A + f(e_x) + g(e_x) = A + e_x > 0, \\ f(e_x) - g(e_x) - e_x = e_x - e_x = 0.\end{cases} \tag{27}$$

If $e_x < 0$, $f(e_x) = 0$, and $g(e_x) = -e_x$, then

$$\begin{cases}A + f(e_x) + g(e_x) = A - e_x > 0, \\ f(e_x) - g(e_x) - e_x = e_x - e_x = 0.\end{cases} \tag{28}$$

Similarly, we have

$$\begin{cases}A + f(e_y) + g(e_y) > 0, \\ f(e_y) - g(e_y) - e_y = 0.\end{cases} \tag{29}$$

Then the time derivative of Γ is always non-positive. Therefore, the whole system is stable.

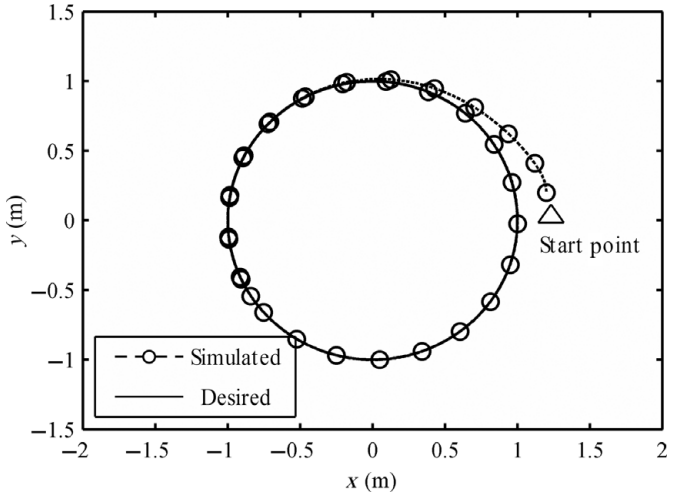


Fig. 6. Spherical robot BHQ-1 tracking a circular trajectory.

4. Simulation and Analysis

Some important parameters of prototype BHQ-1 are listed as follows: the radius R of BHQ-1 is 150 mm; the eccentric mass of BHQ-1 is 800 g; the mass of the spherical shell of BHQ-1 is 152 g and the gross weight of BHQ-1 is 1.8 kg; and the thickness of spherical shell is 2 mm.

In order to validate the effectiveness of the tracking controller, simulations are employed and the tracking simulation results are shown in this section. At last, the analysis of simulation results is presented and a modified control scheme is introduced.

4.1. Tracking a linear trajectory

In this example, the robot is controlled to track a linear trajectory described by

$$\begin{cases}x_d(t) = 0.707t \\ y_d(t) = 0.707t\end{cases}, \quad x_d(0) = y_d(0) = 0. \tag{30}$$

The linear trajectory starts from point (0, 0) in a world coordinate frame and the orientation of this straight line is 45°. The initial configuration of the robot is

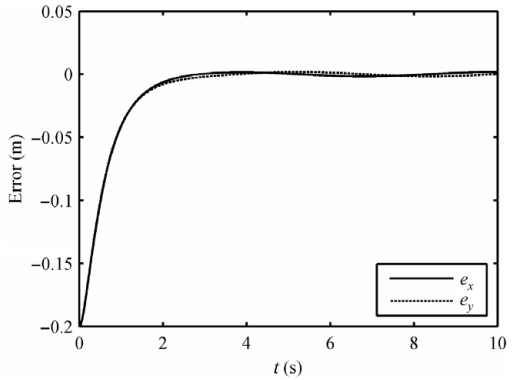
$$\boldsymbol{p}_0 = [x_0, y_0, \psi_0, \beta_0, \varphi_0]^T = [0.2, 0, -\pi/4, 0, 0]^T.$$

The parameters in the shunting equation, i.e., Eq. (19) are $A = 10$, $B = D = 15$. Actually, these parameters can be chosen in a wide range due to the characteristics of the shunting model. For this example, the combination of the parameters selected herein could provide a better tracking performance.

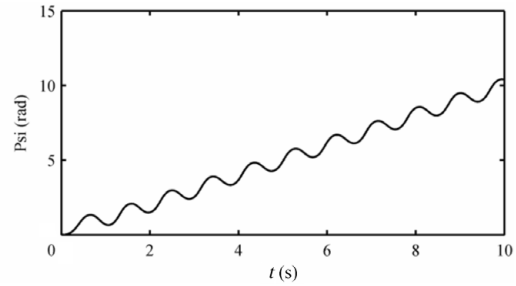
The trajectory tracking simulation is shown in Fig. 4, where the desired trajectory is represented by a solid line and the simulated trajectory is represented by a dashed line with circles.

As demonstrated in Fig. 5(a), the tracking errors are quickly convergent toward zero; Figs. 5(b) and (c) indicate the variation of the attitude angles ψ and β, respectively; the driving speed ϕ' and the steering speed β' are shown in Figs. 5(d) and (e), respectively.

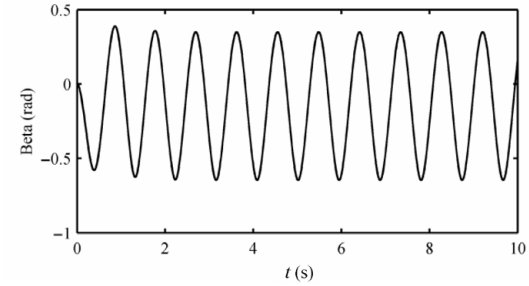
https://doi.org/10.1017/S0263574711000518 Published online by Cambridge University Press



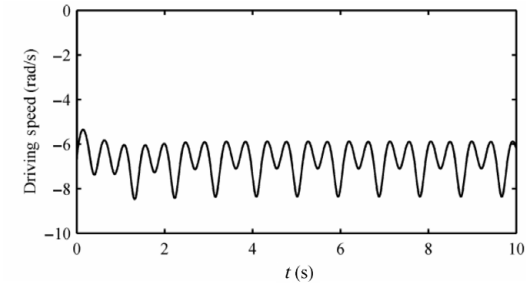
(a) Tracking errors e_x, e_y



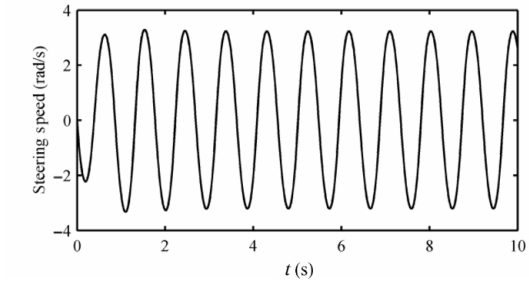
(b) Attitude angle ψ



(c) Attitude angle β



(d) Driving speed φ'



(e) Steering speed β'

Fig. 7. Tracking errors, attitude angles, and velocities for a circular trajectory.

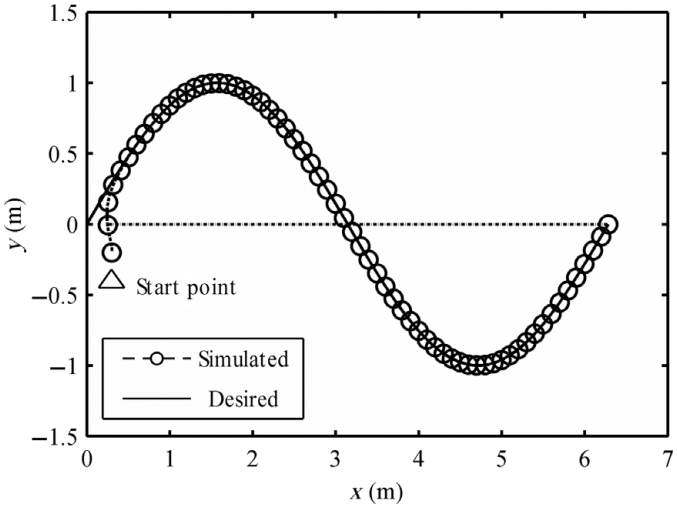


Fig. 8. Spherical robot BHQ-1 tracking a sinusoidal trajectory.

4.2. Tracking a circular trajectory

Consider the robot tracking a circular trajectory described by

$$\begin{cases} x_d(t) = \cos t \\ y_d(t) = \sin t \end{cases}, \quad x_d(0) = 1, \quad y_d(0) = 0. \tag{31}$$

This circle starts from point (1, 0) in a world coordinate frame. Let the initial configuration be

$$p_0 = [x_0, y_0, \psi_0, \beta_0, \varphi_0]^T = [1.2, 0.2, 0, 0, 0]^T .$$

The parameters of the shunting model are $A = 10$, $B = D = 15$.

The result of circular trajectory tracking simulation is shown in Fig. 6, where the desired trajectory is represented by a solid line and the simulated trajectory is represented by a dashed line with circles. The tracking errors, attitude angles, driving speed, and steering speed are shown in Fig. 7.

4.3. Tracking a sinusoidal trajectory

Compared with the linear and circular trajectories, sinusoidal trajectories are more complex and sinusoidal signals are often used in the evaluation of various control systems. A sinusoidal trajectory described by Eq. (32) is considered in this simulation

$$\begin{cases} x_d(t) = 0.1t \\ y_d(t) = \sin(x_d(t)) \end{cases}, \quad x_d(0) = 0, \quad y_d(t) = 0. \tag{32}$$

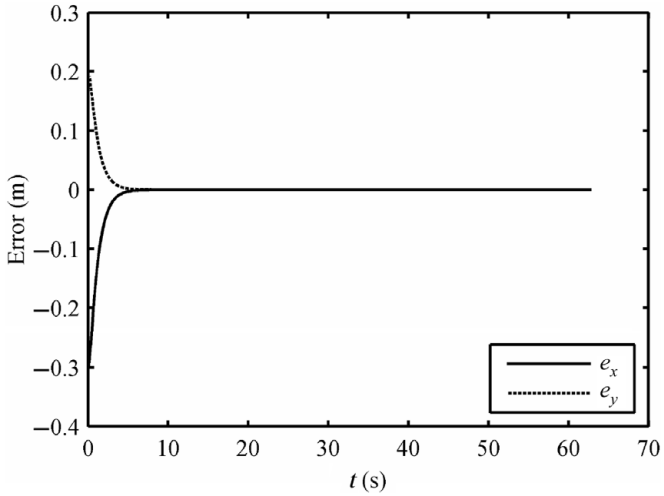
This trajectory starts from point (0, 0). Let the initial configuration be

$$\boldsymbol{p}_0 = [x_0, y_0, \psi_0, \beta_0, \varphi_0]^T = [0.3, -0.2, 0, 0, 0]^T . \tag{33}$$

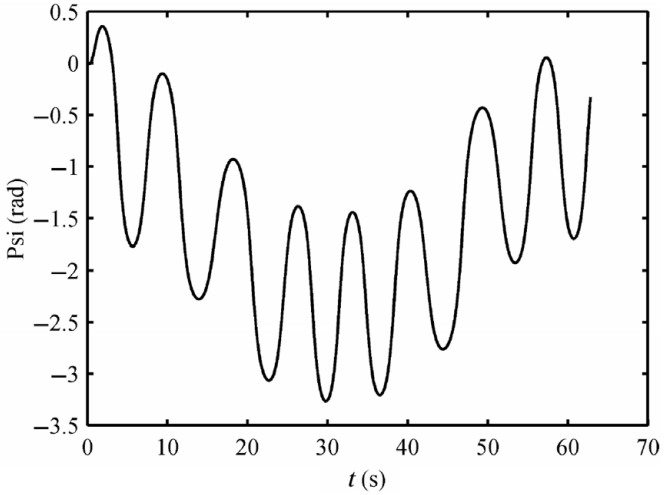
The parameters of the shunting model are $A = 10$, $B = D = 50$.

The simulation result of sinusoidal trajectory tracking is shown in Fig. 8, where the desired trajectory is represented by a solid line and the simulated trajectory is represented by a

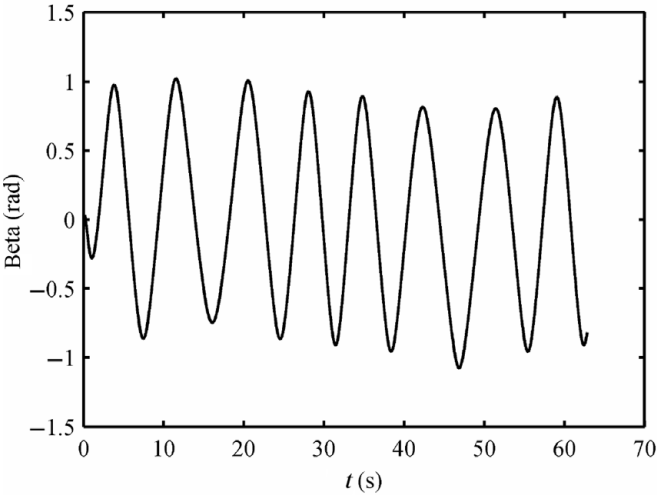
https://doi.org/10.1017/S0263574711000518 Published online by Cambridge University Press



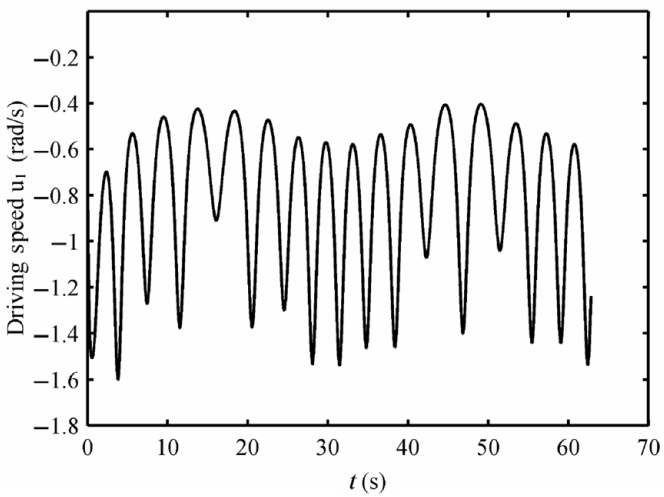
(a) Tracking errors e_x, e_y



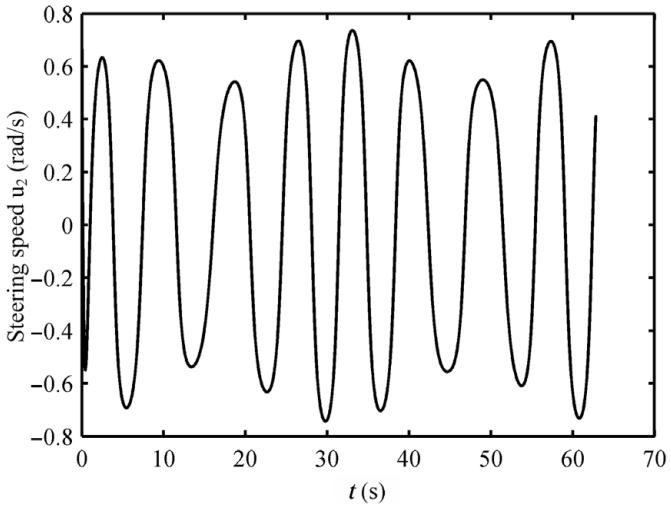
(b) Attitude angle ψ



(c) Attitude angle β



(d) Driving speed φ'



(e) Steering speed β'

Fig. 9. Tracking errors, attitude angles, and velocities for a sinusoidal trajectory.

https://doi.org/10.1017/S0263574711000518 Published online by Cambridge University Press

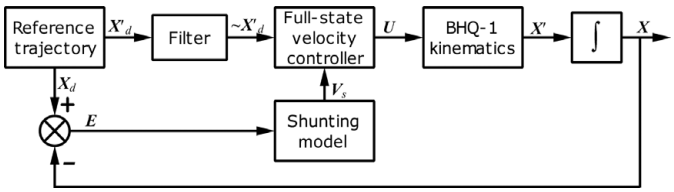


Fig. 10. A modified control scheme of the full-state trajectory tracking controller.

dashed line with circles. The tracking errors, attitude angles, driving speed, and steering speed are shown in Fig. 9.

4.4. Analysis

From simulation results of tracking linear, circular, and sinusoidal trajectories, it can be found that with the proposed controller the robot can track the desired continuous trajectory accurately. The driving speed and steering speed of the robot vary smoothly without sharp jump as $t > 0$. However, there is still an initial speed jump as shown in Figs. 5(d), 7(d), and 9(d); it is because of the existence of a term $\boldsymbol{X}'_d$ in Eq. (16). Besides, although the robot can track the desired trajectory accurately, the two attitude angles ψ and β do not converge to the desired value but vary around that. That's because the two-state tracking controller ignores the orientation of the trajectory and hence can only track the position of the trajectory.

In order to track both the position and orientation, a full-state controller should be considered. For BHQ-1, the full-state tracking means that positions x and y and the poses ψ, β, and φ of the robot can all converge to the desired values. While, a filter can also be introduced to generate the smooth desired velocity for solving the initial speed jump problem and tracking the discontinuous trajectories. A modified control scheme as shown in Fig. 10 will be researched in future, which is more useful for practical applications.

5. Conclusions

Different from classic mobile robots, such as a wheeled robot, spherical robot is a nonchained system. The trajectory tracking control of spherical robot is very useful in practice but very few literatures discuss it. In this paper, the two-state trajectory tracking problem of spherical robot BHQ-1 is studied and a controller based on the Lyapunov's direct method and neurodynamic technique has been proposed. The Lyapunov stability analysis and simulation results show the effectiveness of the proposed controller. At last, a modified control scheme to overcome the shortcomings of the proposed two-state tracking controller has been represented.

A new point in this paper is that, to the best of our knowledge, for the first time a trajectory tracking controller of spherical robot on the basis of kinematic model is proposed. Besides, the kinematic modeling of spherical robot with screw theory and trajectory tracking controller design with neurodynamics can be used to other spherical robots and nonholonomic systems.

Acknowledgments

This work is supported in part by National Natural Science Foundation of China under grant No. 50705003, National High Technology Research and Development Program of China under grant No. 2007AA04Z252, and "Blue Star Program" of Beijing University of Aeronautics and Astronautics.

References

1. R. M. Murray, Z. Li and S. S. Sastry, *A Mathematical Introduction to Robotic Manipulation* (CRC Press, Boca Raton, Florida, 1994).
2. Z. Li and J. Canny, "Motion of two rigid bodies with rolling constraint," *IEEE Trans. Rob. Automat.* **6**(1), 62–72 (1990).
3. T. Das and R. Mukherjee, "Exponential stabilization of the rolling sphere," *Automatica* **40**(Jun), 1877–1889 (2004).
4. T. Das and R. Mukherjee, "Reconfiguration of a rolling sphere: A problem in evolute-involute geometry," *ASME J.Appl. Mech.* **73**(Jul), 590–597 (2006).
5. A. H. A. Javadi and P. Mojabi, "Introducing August: A Novel Strategy for an Omnidirectional Spherical Rolling Robot," *Proceedings of the IEEE International Conference on Robotics and Automation*, Washington DC, USA, (May 2002), pp. 3527–3533.
6. S. Bhattacharya and S. K. Agrawal, "Spherical rolling robot: A design and motion planning studies," *IEEE Trans. Rob. Automat.* **16**(Dec), 835–839 (2000).
7. A. Halme, T. Schonberg and Y. Wang, "Motion Control of a Spherical Mobile Robot," *Proceedings of Advanced Motion Control*, Tsu-City, Japan (1996), Vol. 1, pp. 259–264.
8. A. Halme, J. Suromela, T. Schonberg and Y. Wang, "A Spherical Mobile Microrobot for Scientific Applications," Proceedings of *ASTRA96*, ESTEC, Noordwijk, The Netherlands (Nov. 6–7, 1996).
9. A. Bicchi, A. Balluchi, D. Prattichizzo and G. Andrea, "Introducting the 'Sphericle': An Experimental Testbed for Research and Teaching in Nonholonomy," *International Conference on Robotics and Automation*, Albuquerque, NM, USA (Apr. 1997) Vol. 3, pp. 2620–2625.
10. A. Bicchi and A. Marigo, "A Local–Local Planning Algorithm for Rolling Objects," *Proceedings of the 2002 IEEE International Conference on Robotics and Automation*, Washington, USA (May 2002) Vol. 2, pp. 1759–1764.
11. V. A. Joshi, R. N. Banavar and R. Hippalgaonkar, "Motion analysis of a spherical mobile robot," *Robotica* **27**, 243–353 (2009).
12. V. A. Joshi, R. N. Banavar and R. Hippalgaonkar, "Design and analysis of a spherical mobile robot," *Mechanism and Machine Theory* **45**(2), 130–136 (2010).
13. D. Liu, H. Sun and Q. Jia, "A Family of Spherical Mobile Robot: Driving Ahead Motion Control by Feedback Linearization," *2nd International Symposium on Systems and Control in Aerospace and Astronautics*, Shenzhen, China, (Dec. 12, 2008) pp. 1–6, 10–12.
14. Q. Zhan, C. Jia, X. Ma, Y. Zhai, "Mechanism design and motion analysis of a spherical mobile robot," *Chinese J. Mech. Eng.* **18**(4), 542–545 (2005).
15. H. Yang, "Tracking Control of a Nonholonomic Mobile Robot by Hybrid Feedback and Neural Dynamics Techniques," Master's thesis, University of Guelph for Engineering (2004).
16. A. L. Hodgkin and A. F. Huxley, "A quantitative description of membrane current and its application to conduction and excitation in nerve," *J. Phys.* **117**, 500–544 (1952).
17. S. Grossberg, "Nonlinear neural networks: Principles, mechanism and architectures," *Neural Netw.* **1**, 17–61 (1988).
18. A. Isidori, *Nonlinear Control Systems*, 3rd ed (Springer, Berlin, 1955).

https://doi.org/10.1017/S0263574711000518 Published online by Cambridge University Press